2684 *Inorg. Chem.* **2010**, *49*, 2684–2691
DOI: 10.1021/ic902403f

Inorganic Chemistry
Article

Simple and Efficient Synthesis of a Nd:$LaAlO_3$ NIR Nanophosphor from Rare Earth Alkoxo-Monoaluminates $Ln_2Al_2(O^iPr)_{12}(^iPrOH)_2$ Single Source Precursors by Bradley Reaction

Robert Pazik,[†] Gulaim A. Seisenbaeva,[†] Suresh Gohil,[†] Rafal Wiglusz,[‡] Leszek Kępiński,[‡] Wieslaw Strek,[‡] and Vadim G. Kessler*[,†]

[†]*Department of Chemistry, SLU P.O. Box 7015, 750 07 Uppsala, Sweden, and* [‡]*Institute of Low Temperatures and Structure Research, PAS, Okolna 2, 50-422 Wroclaw*

Received September 13, 2009

Nanoparticles of a Nd-doped $LaAlO_3$ perovskite can be obtained rapidly and with quantitative yield using the Bradley (ether elimination) treatment of a mixture of individual $Ln_2Al_2(O^iPr)_{12}(^iPrOH)_2$, Ln = La, Nd, in acetophenone. The initially produced particles are poorly crystalline, but their crystallinity improves strongly on heating to 800 °C, which leads also to a controllable aggregation. The prepared nanoparticles are rather solution stable and can easily be surface-modified, which opens prospects for their use as phosphors in bioimaging applications. The precursors, bimetallic isopropoxides of rare earth elements and aluminum with a 1:1 composition, $Ln_2Al_2(O^iPr)_{12}(^iPrOH)_2$, can be prepared with high yields via direct dissolution of metallic lanthanoids in a solution of aluminum isopropoxide in a toluene−isopropanol medium or through a short time reflux of "$Ln(O^iPr)_3$" with 1 equiv of $Al(O^iPr)_3$ in toluene. In spite of good volatility and their proper composition, the $Ln_2Al_2(O^iPr)_{12}(^iPrOH)_2$, Ln = La, Nd, do not act as single-source precursors in MOCVD, because of their quantitative transformation into $LnAl_3(O^iPr)_{12}$ together with $Ln_5O(O^iPr)_{13}$ on evaporation. These molecules are, however, present intact in solution according to variable temperature NMR studies, which permits application of them successfully as single source precursors in the synthesis of Ln:$LaAlO_3$ perovskite nanopowders with compositions thoroughly controlled through the conditions of the synthesis. Luminescent properties of the Nd:$LaAlO_3$ were examined and discussed in detail. The thermal population of the $^4F_{5/2}$ and $^2H_{9/2}$ states was found as a consequence of the grain size effect causing difficulties in heat dissipation. Moreover, luminescence behavior of the powder annealed at a lowest temperature shows well-defined short-range order.

Introduction

The interest in NIR nanophosphors in bioimaging applications is due, on one hand, to the possibility of achieving their excitation with a light having a wavelength within the visible region and thus being harmless for the illuminated tissues.[1] Another important advantage of these materials lies in their ability to transfer light into heat and thus act as triggers of heat-related delivery of medicines.[2] Preparation of highly phase pure uniform-size $LaAlO_3$ perovskite nanopowders that can serve as a host for luminescent doping is a considerable challenge.[3] Ideal perovskite with the ABO_3 chemical formula has a cubic structure with $Pm\bar{3}m$ symmetry. However, the $LaAlO_3$ is rhombohedral with space group $R\bar{3}c$ at room temperature. The rhombohedral distortion is very low and can be described as a rotation of the O_6-octahedron expressed by one x(O) parameter.[4,5] The lanthanide ion occupies the D_3 point symmetry site and is coordinated by 12 oxygen ions, which results in only one site under a magnetic field. As a consequence, the structure of the $LaAlO_3$ is often described in the literature as pseudocubic which undergoes phase transition at 527 °C into an ideal cubic perovskite structure.

The hydrolytic approach to perovskite $LnAlO_3$ materials has been discussed directly after the discovery of the first representative of the potential single-source precursor family, $Er_2Al_2(O^iPr)_{12}(^iPrOH)_2$,[6] in 1998. The first report on the

*To whom correspondence should be addressed. E-mail: vadim.kessler@kemi.slu.se.

(1) le Masne de Chermont, Q.; Chaneac, C.; Seguin, J.; Pelle, F.; Maîtrejean, S.; Jolivet, J.-P.; Gourier, D.; Bessodes, M.; Scherman, D. *Proc. Natl. Acad. Sci. U.S.A.* **2007**, *104*, 9266.
(2) Yong, K. T.; Roy, I.; Swihart, M. T.; Prasad, P. N. *J. Mater. Chem.* **2009**, *19*, 4655.
(3) Yu, H. F.; Wang, J.; Wang, S. S.; Kuo, Y. M. *J. Phys. Chem. Solids* **2009**, *70*, 218.
(4) Howard, C. J.; Kennedy, B. J.; Chakoumakos, B. C. *J. Phys.: Condens. Matter* **2000**, *12*, 349.
(5) Geller, S.; Raccah, P. M. *Phys. Rev. B* **1970**, *2*, 1167.
(6) Kritikos, M.; Wijk, M.; Westin, G. *Acta Crystallogr., Sect. C* **1998**, *54*, 576.

 Published on Web 02/08/2010

morphology and phase composition of the related nanopowders appeared only in 2004 and dealt with application of $Y_2Al_2(O^iPr)_{12}(^iPrOH)_2$.[7] The powders of otherwise thermodynamically unstable $YAlO_3$ have been successfully obtained, but the particles in them were strongly aggregated, hindering, together with the phase instability of this matrix, its application as a potential host of a NIR phosphor. Major interest in the development of other representatives in this precursor family was put then on their use in liquid-assisted MOCVD synthesis of perovskite rare earth aluminate coatings. Both neodymium[8,9] and lanthanum and praseodymium[9,10] derivatives have been studied, but it turned out that the application of these single molecular sources was associated with a partial loss of the rare earth component. This feature in the precursor behavior was not understood earlier and could even be considered as a sign of potential difficulties in their application even for the production of nanopowders by the spray-pyrolysis technique and even by sol−gel. Another hindrance in the development of application for this class of compounds has been their quite complex synthesis. They were obtained through either interaction of anhydrous rare earth chloride with potassium alkoxide in an alcohol/hydrocarbon medium with a subsequent addition of aluminum alkoxide[6,9,10] or through an even much more complex procedure, where t-butoxide derivatives of the two metals were first produced independently and then reacted with each other and the product of their reaction subjected further to alcohol interchange to provide the desired isopropoxide complex.[7,8] In the present contribution, we describe the use of principally simpler and more efficient synthetic approaches, the stability studies for this class of precursors in the gas phase by mass-spectrometry and in solution by variable temperature NMR, and also their successful application in the synthesis of highly solution stable nanoparticles of lanthanide doped lanthanum aluminate, which is attractive as a NIR emitting phosphor.

Experimental Section

All manipulations with precursor chemicals were carried out in a dry nitrogen atmosphere using Schlenk techniques or a glovebox if not otherwise specified. Isopropanol and *n*-propanol (Merck, p.a.) were purified by distillation over corresponding $Al(O^iPr)_3$, and hexane and toluene (Merck, p.a.) were purified by distillation over $LiAlH_4$. IR spectra of nujol mulls were registered with a Perkin-Elmer FT-IR Spectrum 100 spectrometer. NMR spectra were recorded for the precursors as $CDCl_3$ solutions and for the nanoparticles as D_2O solutions on a Bruker 400 MHz spectrometer at 30 °C and −20 °C. The X-ray single crystal and powder studies have been carried out with a multipurpose Bruker SMART CCD 1k diffractometer. SMART software was used for the data collection and SAINTPLUS or APEX-2 program packages for the data reduction and integration for the single crystal and powder experiments, respectively. Low temperature single crystal data for $Nd_2Al_2(O^iPr)_{12}(^iPrOH)_2$ were obtained using a Nonius Kappa-CCD diffractometer at the Royal Institute of Technology, Stockholm, Sweden. The satisfactory microanalysis data for the precursor complexes were obtained by Mikro Kemi AB in Uppsala, Sweden.

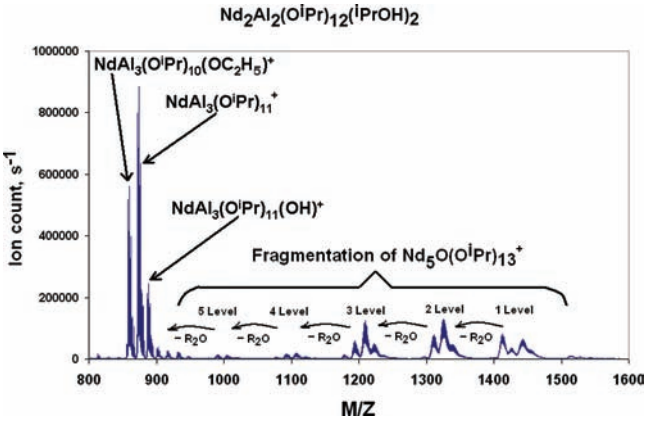

Figure 1. EI mass spectrum of $Nd_2Al_2(O^iPr)_{12}(^iPrOH)_2$ on evaporation in a dynamic vacuum. Presented high mass region includes 5 levels of $Nd_5O(O^iPr)_{13}$ fragmentation, but only the first mass level for the $NdAl_3(O^iPr)_{12}$ fragmentation is covered.

Mass-spectra were recorded using a JEOL JMS-SX/SX-102A mass-spectrometer applying electron beam ionization (U = 70 eV) with direct probe introduction. The evaporation in a dynamic vacuum was studied applying the recently developed multivariate analysis technique, establishing the correlation between the total ion current and ion currents corresponding to the well-identified fragments, corresponding to the molecular forms present in the gas phase.[11]

The XPD patterns were collected at room temperature on a Stoe STADI P transmission diffractometer in Debye−Scherrer geometry (Cu $K\alpha_1$: 1.54060 Å) equipped with a linear position sensitive detector and on the SMART CCD 1k diffractometer using Mo Kα radiation (0.71073 Å). The $LaAlO_3$ powders were investigated by transmission electron microscopy (TEM) using a Philips CM-20 SuperTwin microscope, operating at 200 kV. Specimens for HRTEM were prepared by dispersing a powder sample in methanol and putting a droplet of the suspension on a copper microscope grid covered with perforated carbon. Elemental analysis of powders was performed utilizing a SEM-EDS Hitachi TM-1000-μDeX Tabletop Microscope carrying out for each sample 10 measurements from different randomly distributed areas. The luminescence spectra were recorded using a Jobin Yvon THR1000 monochromator equipped with a Hamamatsu R406 photomultiplier and a 1200 grooves/mm holographic grating. As an excitation source, a continuous 514.8 nm line of the Ar^+ laser was used. The lifetimes were measured utilizing an OPO (optical parametric oscillator) pumped by the third harmonics of a Nd:YAG laser with a 10 ns pulse. Raman spectroscopy was done using a LabRam HR 800 Horiba Yvon Jobin equipped with a 9 mW HeNe laser emitting a 632.8 nm line. All recorded spectra were corrected according to the apparatus characteristics.

Precursor Synthesis. The preparation of heterometallic precursors was carried out by refluxing, over 15 min, equivalent amounts (about 2 g in total) of "$Ln(O^iPr)_3$" and $Al(O^iPr)_3$ (both purchased from Aldrich and used without any further purification) in a mixture of toluene and isopropanol (3:1 by volume) with subsequent recrystallization from the mother liquor in a freezer at −20 °C overnight. Another approach consisted of refluxing about 1 g of chips of a rare earth metal

(7) Mathur, S.; Shen, H.; Rapalaviciute, R.; Kareiva, A.; Donia, N. *J. Mater. Chem.* **2004**, *14*, 3259.
(8) Mathur, S.; Veith, M.; Shen, H.; Hufner, S.; Jilavi, M. H. *Chem. Mater.* **2002**, *14*, 568.
(9) Gaskell, J. M.; Przybylak, S.; Jones, A. C.; Aspinall, H. C.; Chalker, P. R.; Black, K.; Potter, R. J.; Taechakumput, P.; Taylor, S. *Chem. Mater.* **2007**, *19*, 4796.
(10) Gaskell, J. M.; Jones, A. C.; Aspinall, H. C.; Przybylak, S.; Chalker, P. R.; Black, K.; Davies, H. O.; Taechakumput, P.; Taylor, S.; Critchlow, G. W. *J. Mater. Chem.* **2006**, *16*, 3854.
(11) Kessler, V. G.; Seisenbaeva, G. A.; Gohil, S. *Surf. Coat. Technol.* **2007**, *201*, 9082.

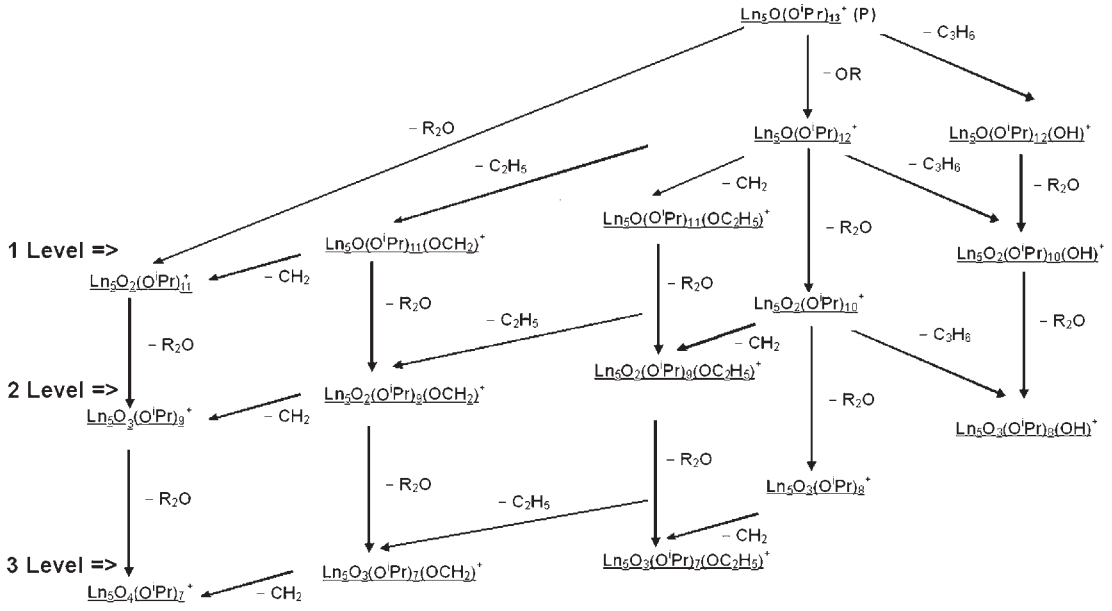

Figure 2. Fragmentation tree of the $Ln_5O(O^iPr)_{13}$ complexes with identification of the individual fragments within first, second, and third mass levels.

together with 1 equiv of $Al(O^iPr)_3$ in the same medium until complete dissolution, adding a crystal of solid iodine or $HgCl_2$ for initiation of the reaction. The typical yields were between 80 and 90% in relation to the rare earth source. The spectral characteristics of the obtained precursors corresponded to those reported in refs 8−10.

Crystallography. Data collection was run for the unit cell parameter determination randomly for 6−8 samples from each synthesis batch to identify the crystalline phase. A complete data collection has been carried out for one single crystal of each compound. The structures were solved by direct methods. The coordinates of the rare earth metal atoms were obtained from the initial solution, and the coordinates of all other non-hydrogen atoms were found in the subsequent Fourier syntheses. The coordinates of all non-hydrogen atoms were refined first in isotropic and then in anisotropic approximations. The coordinates of the hydrogen atoms were calculated geometrically and included into the final refinement in isotropic approximation using the rider model.

Synthesis of Nanoparticles. In order to prepare the $LaAlO_3$ nanoparticles doped with 2 mol % of Nd^{3+} ions, 0.2 g (0.172 mmol) of $La_2Al_2(O^iPr)_{12}(^iPrOH)_2$ and 4.03 mg (0.00344 mmol) of $Nd_2Al_2(O^iPr)_{12}(^iPrOH)_2$ precursors were dissolved in 25 mL of acetophenone, resulting in a transparent yellow solution at room temperature. The prepared solution was refluxed at 202 °C for 8 h until the turbid yellow suspension was formed. The final product was separated by high speed centrifugation and further washed by absolute ethanol portions of 10 mL six times for removal of the acetophenone. Afterward, the particles were suspended in a fresh portion of absolute ethanol and dried using a vacuum evaporator. Additional thermal treatment (500−1000 °C for 8 h) was applied in order to improve the crystallinity of the particles and to control their grain size. The same procedure was applied also for preparation of $LaAlO_3$ nanoparticles doped with 1, 5, and 10 mol % of Nd^{3+} ions (using corresponding amounts of alkoxide precursors).

Results and Discussion

The preparation of the $Ln_2Al_2(O^iPr)_{12}(^iPrOH)_2$, Ln = La, Nd, happened to be an extremely facile and easily reproducible procedure. We have turned then to the studies of stability of these derivatives. All the representatives of this series are appreciably volatile, providing highly intensive and strikingly analogous EI mass spectra.

In the process of obtaining an EI mass spectrum using a direct insertion probe, the gas phase molecule of the title compound ($Ln_2Al_2(O^iPr)_{12}(^iPrOH)_2$) gives rise to two species, namely, $Ln_5O(O^iPr)_{13}$ and $LnAl_3(O^iPr)_{12}$. Although the molecular ion (P^+), $(P-CH3)^+$, and $(P-H)^+$ are of negligible intensities, nevertheless $(P-O^iPr)^+$ could be detected and starting from this fragment ion the pattern in the resulting mass spectrum can be explained in terms of two major pathways, namely elimination of a neutral molecule of propene (C_3H_6) to give a -OH function and/or elimination of diisopropyl ether (R_2O).[12,13]. These sequential stepwise products of mass fragmentation are depicted in Figure 2. The other ions in the spectrum, possibly formed by rearrangements in the isopropyl group, are assigned tentatively and the compositions are as noted in Figures 1 and 3. The relative intensity of each distinct fragment in the spectrum is related to both its thermodynamic and kinetic stability toward further fragmentation, which provides a basis for the creation of mass-spectral databases for identification of individual compounds in a mixture through their fragmentation pattern.[14] The spectra of the complexes with a Ln/Al = 1:1 composition (see Figure 1 and FS1-FS4) have surprisingly demonstrated very distinctly the combination of fragmentation patterns characteristic of homometallic $Ln_5O(O^iPr)_{13}$ (see Figure 2 for the complete fragmentation scheme for this class of complexes) in combination with those of bimetallic complexes with a Ln/Al = 1: 3 composition, $LnAl_3(O^iPr)_{12}$.

Even in the spectra of the Nd complex, where the picture is partly complicated by the complex isotope composition for this element (7 stable isotopes with comparable abundance, ^{142}Nd 27.13%, ^{143}Nd 12.18%, ^{144}Nd 23.80%, ^{145}Nd 8.30%,

(12) Turova, N. Ya.; Turevskaya, E. P.; Kessler, V. G.; Yanovkaya, M. I. *The Chemistry of Metal Alkoxides*; Kluwer, AP: Boston, 2002.
(13) Suslova, E. V.; Kessler, V. G.; Gohil, S.; Turova, N. Ya. *Eur. J. Inorg. Chem.* **2007**, 5182.
(14) (a) Yates, J. R. *Electrophor.* **1998**, *19*, 893. (b) Lahm, H. W.; Langen, H. *Electrophor.* **2000**, *21*, 2105.

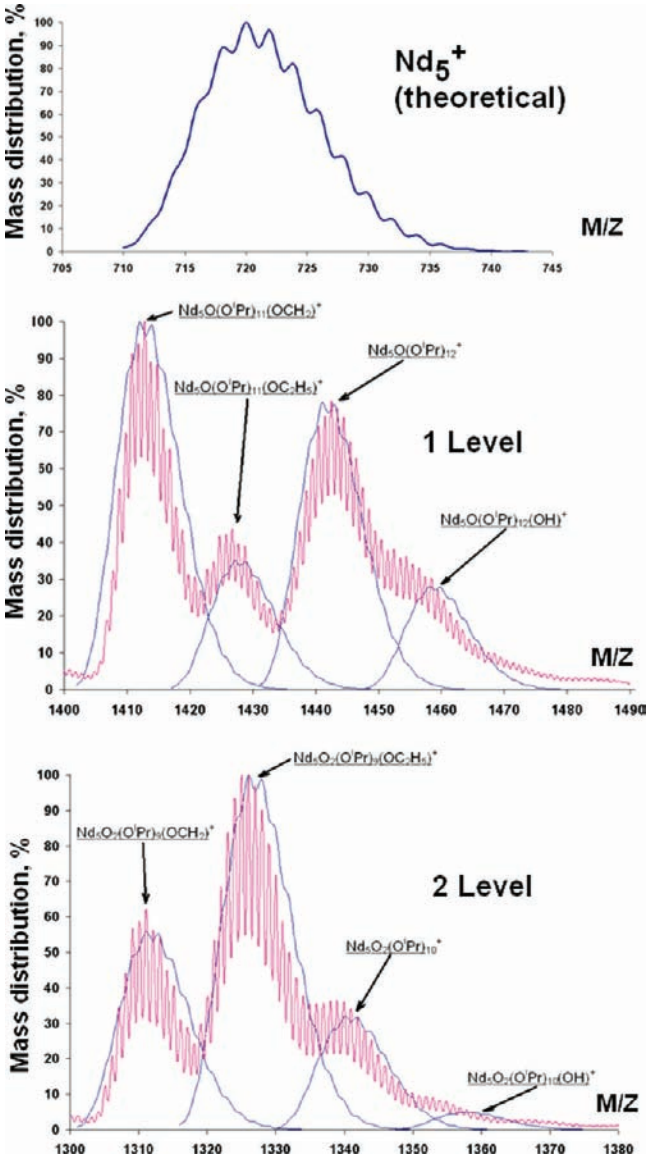

Figure 3. Theoretical shape of the Nd_5-core isotope profile and comparison of the observed spectra with theoretical mass distributions within the first and second mass levels for the fragmentation of $Nd_5O(O^iPr)_{13}$.

^{146}Nd 17.19%, ^{148}Nd 5.76%, and ^{150}Nd 5.64%) all individual fragments could be unequivocally identified and interpreted.

The isotope profile for a molecule with 5 neodymium atoms is thus a typical random statistical distribution (a Gaussian-like curve). Applying the Sheffield Chemputer Program,[15] providing the isotope distribution for individual fragments, we were even able to model the observed intensity distributions within individual mass levels of the fragmentation pattern of $Nd_5O(O^iPr)_{13}$ (see Figure 3).

This indicated that a complete transformation of $Ln_2Al_2(O^iPr)_{12}(^iPrOH)_2$ into the two types of species $Ln_5O(O^iPr)_{13}$ and $LnAl_3(O^iPr)_{12}$ occurred on evaporation. Direct confirmation of this conclusion was obtained by the multivariate analysis of the evaporation in a dynamic vacuum. The total ion current profile indicated that the evaporation process started with elimination of the solvating alcohol,

(15) Winter, M. J.; Rzepa, H. S.; Whitaker, B. J. *Chem. Brit.* **1995**, *31*, 685. Sheffield ChemPuter. http://winter.group.shef.ac.uk/chemputer/ (accessed Jan 2010).

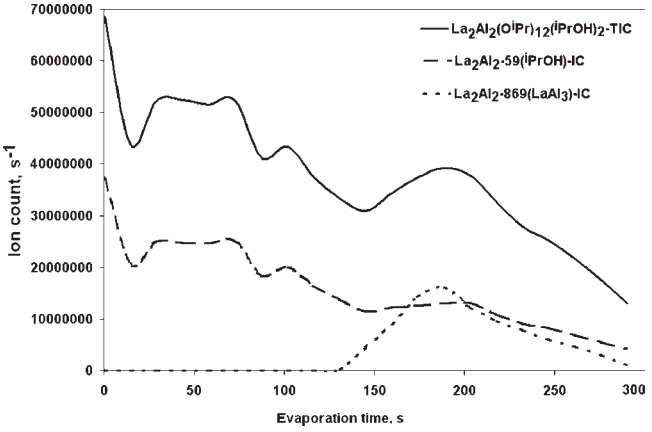

Figure 4. Comparison of the total ion current (TIC) and the ion currents (IC), corresponding to the signals originating from ^{i}PrOH and $LaAl_3(O^iPr)_{12}$, respectively.

followed by release of the more volatile and, due to their lower molecular weights, easier diffusing 1:3 bimetallic species (see Figure 4).

The evaporation of the "single source precursor" was thus in this case associated with the reaction:

$$15Ln_2Al_2(O^iPr)_{12}(^iPrOH)_2 \rightarrow 4Ln_5O(O^iPr)_{13} + 10LnAl_3(O^iPr)_{12} + 4^iPr_2O + 30^iPrOH$$

transforming it in reality into a mixture of two distinct molecular species and thus an *in situ* double source precursor. The stoichiometric ratio between the products should be 4:10. The ratio of intensities in the mass spectrum (sum of ion currents for the observed fragments in the higher mass region, see Figure 1) for neodymium gives an amazingly good correspondence of 4.2:10.0, showing that, with an extremely short diffusion pathway within the ion source volume of the mass spectrometer, the evaporation of the decomposition products is practically complete and follows the reaction stoichiometry. It is fully understandable why the authors of refs 8−10 were convinced that they had a single source precursor situation! The difficulties in keeping the proper ratio between metal atoms in the deposit was caused then apparently by a striking difference in the diffusion coefficients for the two resulting species, $LnAl_3(O^iPr)_{12}$ and $Ln_5O(O^iPr)_{13}$, due to the difference in their molecular mass.

The dissociation or transformation on evaporation in some cases might indicate the possibility of these processes even on dissolution. However, the ^{1}H NMR spectrum for $La_2Al_2(O^iPr)_{12}(^iPrOH)_2$ in $CDCl_3$ is in good agreement with the observed solid state structure, see Figure 5, containing at higher temperatures only two C*H* signals, one corresponding to better resolved ^{i}Pr groups of the alkoxide ligands connected to Al atoms and the other to those from alkoxide and solvating alcohol ligands at the La atoms, in the ideal 4:3 ratio. Cooling to −20 °C leads to splitting of the signal, corresponding to the Al-attached alkoxides into two equally intensive peaks, corresponding to pairs of terminal and bridging OR groups in the involved $Al(OR)_4$ structural units. The signal, corresponding to the OR groups and the solvating alcohol attached to La atoms, remains a single one (even by ^{1}H−^{13}C two-dimensional NMR), while it would already be

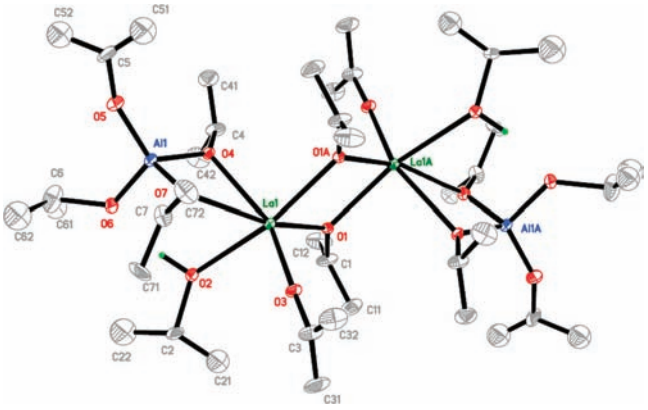

Figure 5. Molecular structure of $La_2Al_2(O^iPr)_{12}(^iPrOH)_2$.

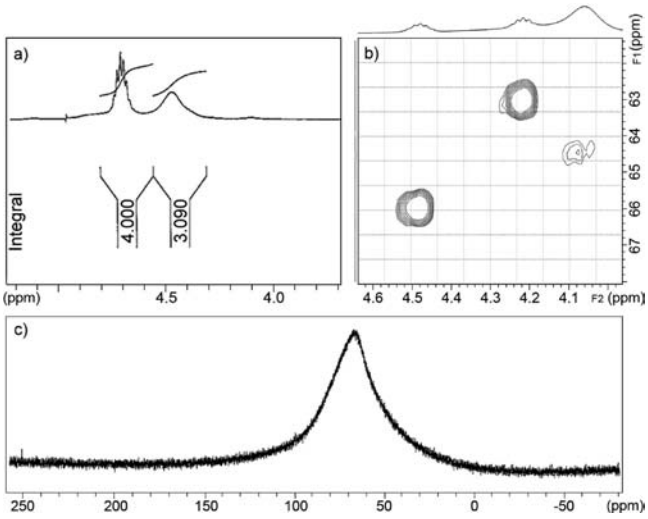

Figure 6. ^1H spectrum at 30 °C (a), $^1H-^{13}C$ correlation spectrum at −20 °C (b), and ^{27}Al NMR spectrum at 30 °C (c) of $La_2Al_2(O^iPr)_{12}(^iPrOH)_2$.

split for the possible admixture of $La_5O(O^iPr)_{13}$ at this temperature.[16] The ^{27}Al NMR spectrum demonstrates one signal, corresponding to tetrahedrally coordinated Al atoms, see Figure 6.

This gave us hope that these precursors could be successfully applied for the synthesis of uniform nanoparticles using the Bradley reaction (ether elimination in a hydrocarbon, alcohol, or carbonyl compound as the solvent).[17−19] Its facility for this class of compounds was demonstrated clearly by the broad representation of this decomposition pathway in the gas phase, according to mass spectra.

The formation of the crystalline Nd:$LaAlO_3$ nanopowders was followed by the XPD measurements (see Figure.7).

The powder derived from the single source alkoxide precursor revealed detectable crystallinity after treatment at 700 °C, while the products obtained directly from the synthesis

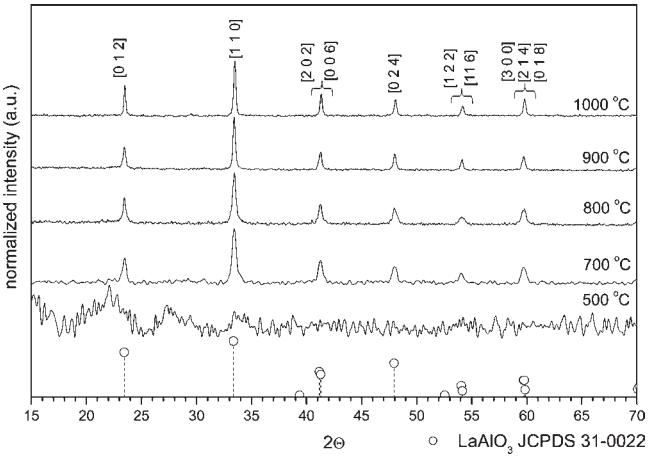

Figure 7. Representative XPD patterns of the Nd:$LaAlO_3$ nanoparticles.

and those sintered at 500 °C remained essentially amorphous in X-rays. The structure corresponds well to the standard $LaAlO_3$ pseudocubic phase.[20] The mean size of crystallites was estimated from the broadening of the diffraction peaks using Scherrer's equation:

$$D = \frac{k\lambda}{\cos\Theta\sqrt{\beta^2 - \beta_0^2}}$$

where D is the grain size, β_0 is the apparatus broadening, β is the full width at half-maximum, Θ is the diffraction angle, k is a constant (usually equal to 0.9), and λ is the X-ray wavelength.[21] Depending on the post-treatment temperature, the average grain size varies from 5 nm up to 40 nm. TEM imaging shows that the Nd:$LaAlO_3$ sample heated at 500 °C (see Figure 8) contains weakly agglomerated irregular particles with a size from 6 to 25 nm.

The particles are often elongated and sometimes form complex, branched structures. Analysis of the SAED pattern from the sample reveals the presence of very broad rings, typical for poorly ordered materials (Figure 8c). The positions of the rings (~0.3 nm and ~0.2 nm) correspond to broad maxima observed in XRD patterns of the samples heated at 500 °C. In addition to broad rings, the SAED patterns also contained individual spots from crystalline particles at positions corresponding to that of cubic $LaAlO_3$. A group of such particles is seen in the upper left part of Figure 8b. As can be seen in Figure 9, some aggregation of the particles occurred, and there are practically no individual particles present for the Nd:$LaAlO_3$ heated at 800 °C.

Instead, there are complex, branched structures. In this case, the SAED pattern contains well developed spotty rings at positions expected for cubic $LaAlO_3$ (Figure 9c). Close examination of an individual aggregate at higher magnification reveals a highly crystalline nature of the particles (Figure 9b and c). Lattice fringes visible in Figure 9b (0.27 nm) correspond to (110) planes of $LaAlO_3$. The formation in the nonhydrolytic synthesis of the nanoparticles with crystalline or at least well ordered cores and a thinner or

(16) Kessler, V. G.; Hubert-Pfalzgraf, L. G.; Halut, S.; Daran, J.-C. *J. Chem. Soc., Chem. Commun.* **1994**, 705.
(17) Bradley, D. C.; Chakravarti, B. N.; Wardlaw, W. J. *J. Chem. Soc.* **1956**, 4439.
(18) (a) Turova, N. Ya.; Kessler, V. G.; Kucheiko, S. I. *Polyhedron* **1991**, *10*, 2617. (b) Kessler, V. G.; Nikitin, K. V.; Belokon', A. I. *Polyhedron* **1998**, *17*, 2309.
(19) Pazik, R.; Tekoriute, R.; Håkansson, S.; Wiglusz, R.; Strek, W.; Seisenbaeva, G. A.; Gun'ko, Y. K.; Kessler, V. G. *Chem.—Eur. J.* **2009**, *15*, 6820.
(20) Card No. 31-0022 JCPDS, International Centre for Diffraction Data **1997.**
(21) Klug, P.; Alexander, L. E. *X-ray Diffraction Procedure*; Wiley: New York, 1954.

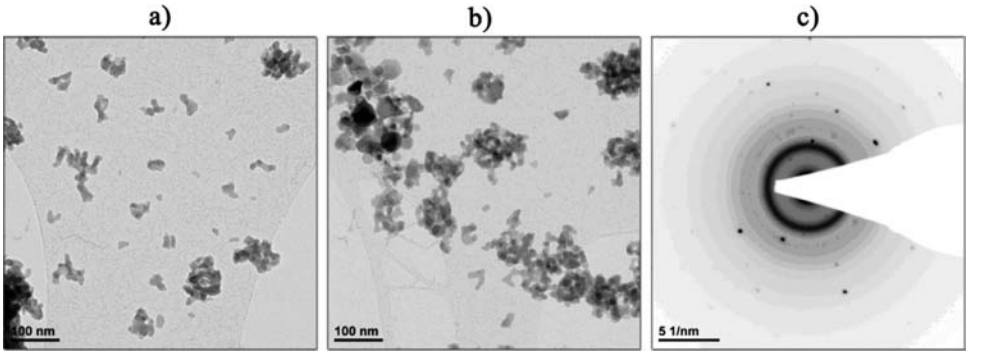

Figure 8. TEM images (a, b) and SAED diffraction (c) of the $LaAlO_3$ heated at 500 °C.

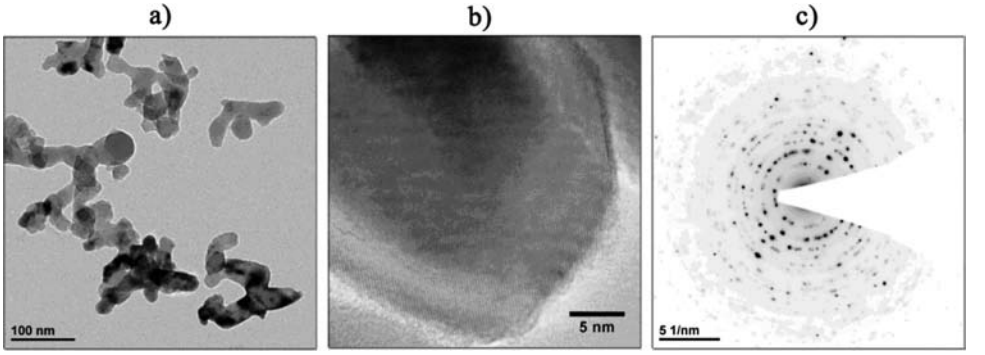

Figure 9. TEM images (a, b) and SAED diffraction (c) of the $LaAlO_3$ heated at 800 °C.

thicker amorphous shell is a very typical feature, originating from the growth mechanism in this case. The nucleation of the particles proceeds via formation of highly ordered polyoxometallate type aggregates formed through coordination equilibrium.[22] They are terminated on the surface by the residual organic ligands. Elimination of the latter leads to formation of an amorphous shell.[23]

The Nd^{3+} content in nanopowders was checked by EDS analysis for the samples produced from precursor mixtures with different neodymium contents varying from 1 mol % to 10 mol % (see Figure 10) with respect to La^{3+}.

The resulting quantity of the Nd^{3+} ions in the $LaAlO_3$ matrix matches truly perfectly with the added amount of the Nd^{3+} ions from the source bimetallic compound $Nd_2Al_2(O^iPr)_{12}(^iPrOH)_2$. Observed small deviations from the assumed dopant content are well within the statistical standard deviations of the EDS analysis, but minor variation of homogeneous distribution of the dopant within the nanoparticle cannot be excluded. Therefore, one could expect that this effect will affect the luminescence properties of the designed system causing formation of the $Nd^{3+}-Nd^{3+}$ pairs and as a consequence quenching of the luminescence by the cross relaxation mechanism.[24] The linear fit parameters for the Nd^{3+} concentration dependence (slope, 1.13 and intercept at 0.02 with R^2, 0.99) show that the incorporation of the dopant from the Nd^{3+} source precursor into the $LaAlO_3$ matrix occurs quantitatively during the synthesis. This means that it is possible to prepare the final material with a broad range of the dopant concentration using as a source compound bimetallic complexes of lanthanum and neodymium with aluminum. The morphology and granulometry of the prepared powders is apparently insensitive to the neodymium content in view of the close chemical analogy in both the precursor complexes and the produced material.

Results of the Raman spectroscopy (see Figure 11) revealed the presence of typical modes of $LaAlO_3$ appearing at 34 cm^{-1} and 125 cm^{-1} (both A_{1g}) and two characteristic shoulders at 155 cm^{-1} and 488 cm^{-1} (both E_{1g}), respectively, confirming the structural purity of prepared materials.[25]

Additionally, we can observe the dominating, over all other bands, electron transitions of the Nd^{3+} (high energetic spectral region), being the result of the applied excitation source used for the Raman measurement.

The reflectance absorption spectra were measured at room temperature covering the typical spectral region of the Nd^{3+} electron transitions (300 nm−800 nm). As a matter of fact, all of them, independently in the thermal treatment, showed the same characteristic Stark splitting of the 4f levels of Nd^{3+}, degenerated by the crystal field. The most intense, among the others, were $^4I_{9/2} \rightarrow {}^4D_{1/2}$, $^2L_{15/2}$ (340 nm); $^4I_{9/2} \rightarrow {}^4G_{5/2}$, $^2G_{7/2}$ (585 nm); $^4I_{9/2} \rightarrow {}^4S_{3/2}$, $^4F_{7/2}$ (740 nm); and $^4I_{9/2} \rightarrow {}^4F_{5/2}$, $^2H_{9/2}$ (800 nm), respectively.

Luminescence spectra of the $LaAlO_3$ doped with 2% Nd^{3+} were measured at 300 and 77 K as function of the sintering temperature 700−1000 °C (see Figures 12 and 13).

The most intense luminescence of the Nd^{3+} originates from the de-excitation of the $^4F_{3/2}$ multiplet. In general, the results are consistent with those reported by Strek et al.[26] for nanopowders of the Nd^{3+} doped $LaAlO_3$ obtained by the

(22) Kessler, V. G. *J. Sol-Gel Sci. Tech.* **2009**, *51*, 264.
(23) Kessler, V. G.; Spijksma, G. I.; Seisenbaeva, G. A.; Håkansson, S.; Blank, D. H. A.; Bouwmeester, H. J. M. *J. Sol-Gel Sci. Tech.* **2006**, *40*, 163.
(24) Powell, R. C. *Physics of Solid-State Laser Materials*; Springer: New York, 1988; p 335.
(25) Scott, J. F. *Phys. Rev.* **1969**, *183*, 823.
(26) Strek, W.; Hreniak, D.; Bednarkiewicz, A.; Mazur, P.; Dereń, P.; Lojkowski, W. *Proc. SPIE* **2004**, *5508*, 240.

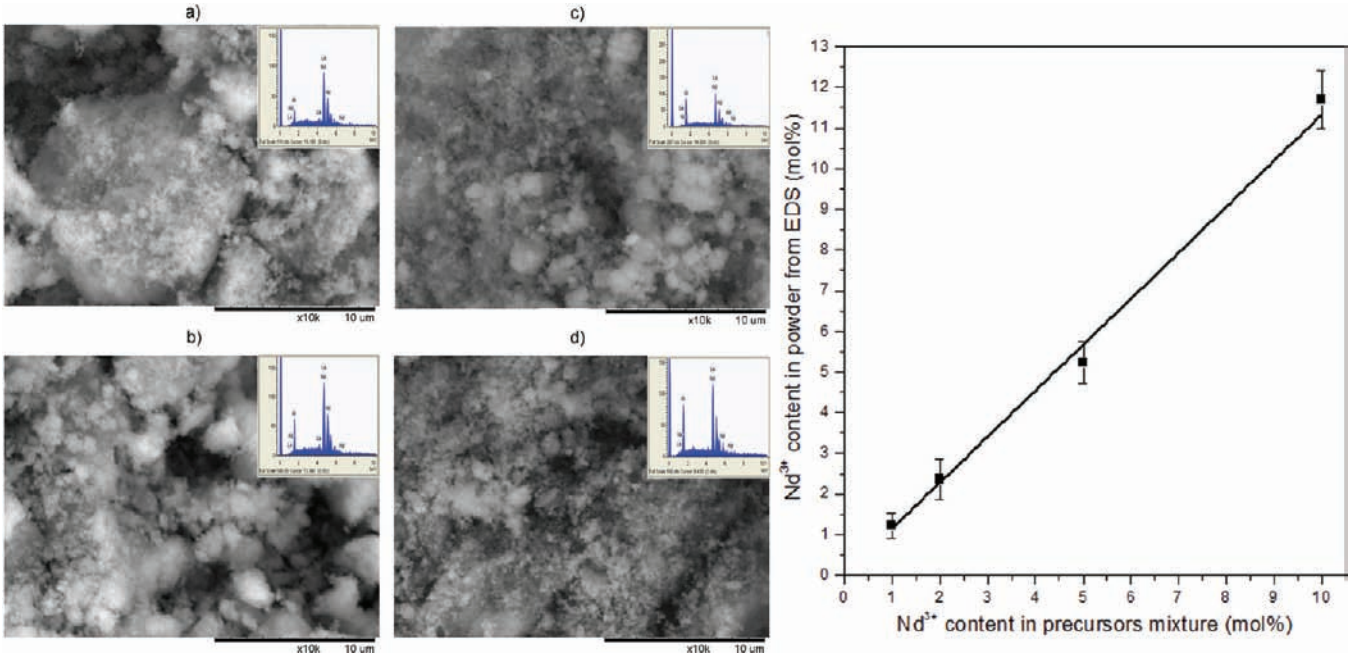

Figure 10. Results of SEM-EDS characterization of Nd:$LaAlO_3$ nanoparticles with various Nd^{3+} concentrations (1−10 mol %).

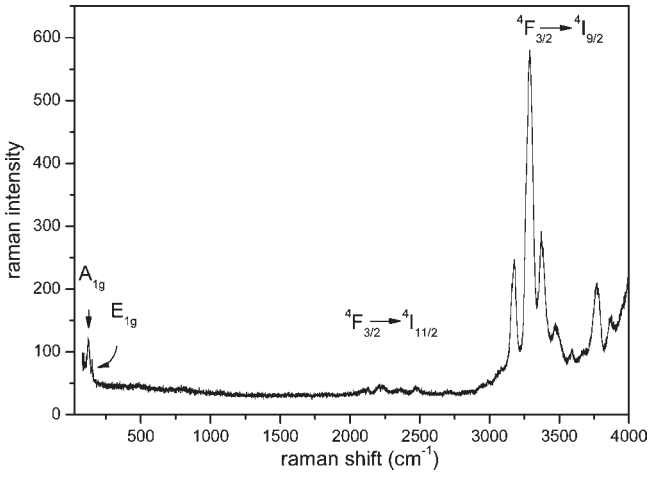

Figure 11. Room temperature Raman spectra of the Nd:$LaAlO_3$ heated at 900 °C.

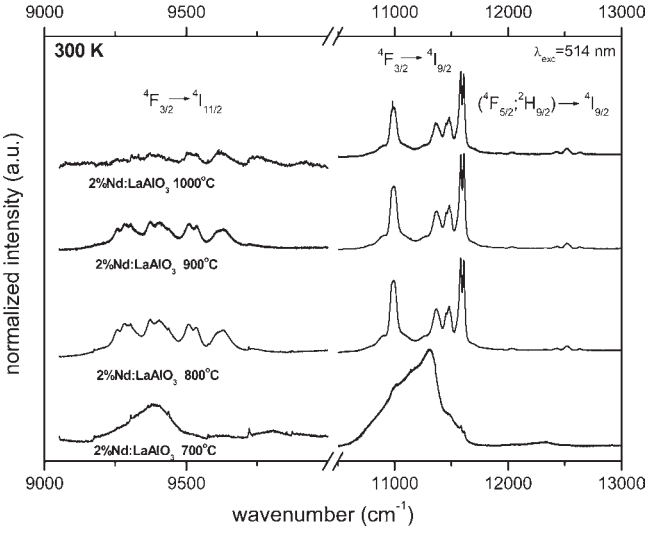

Figure 12. Luminescence spectra of the Nd:$LaAlO_3$ recorded at 300 K as a function of the sintering temperature.

modified Pechini method. The comparison of the luminescence behavior of the Nd:$LaAlO_3$ single crystals described in detail by Dereń et al.[27] revealed the significant difference in the intensity ratio of the $^4F_{3/2}\rightarrow{}^4I_{9/2}$ and $^4F_{3/2}\rightarrow{}^4I_{11/2}$. The former one in our paper is dominating over the $^4F_{3/2}\rightarrow{}^4I_{11/2}$, whereas the intensity of both electron transitions for the Nd:$LaAlO_3$ single crystal have comparable intensities. One can explain it by the higher rhombohedral distortion in case of the $LaAlO_3$ nanopowders. This probably implies that the preferred energy distribution channel is the $^4F_{3/2}\rightarrow{}^4I_{9/2}$ transition instead of $^4F_{3/2}\rightarrow{}^4I_{11/2}$ in our samples. Another interesting feature was the appearance at room temperature of hot emission bands associated with the $(^4F_{5/2}, {}^2H_{9/2})\rightarrow{}^4I_{9/2}$ transitions whose intensities decreased with the increase in sintering temperature. Generally, this effect can be directly connected with the weak heat dissipation of the individual nanocrystals causing the thermal population and emission from higher laying energy levels.[28,29] Moreover, the intensity decrease of these bands with a mutual increase of the sintering temperature points to the grain growth and/or aggregation process, both enhancing the thermal energy dissipation from nanocrystals. Therefore, it finally results in attenuation of the hot-emission processes from the $^4F_{5/2}$ level. One can note that the spectra of the Nd:$LaAlO_3$ sintered at 700 °C at room temperature contains only very broad emission bands, being characteristic for the presence of an amorphous phase. Moreover, at 77 K, we can clearly observe two distinct and thick Stark components of the $^4F_{3/2}\rightarrow{}^4I_{9/2}$ electron transition. It points to the presence of the short-range order within the

(27) Dereń, P. J.; Bednarkiewicz, A.; Goldner, Ph.; Guillot-Noel, O. *J. Appl. Phys.* **2008**, *103*, 043102.

(28) Hreniak, D.; Strek, W. *J. Alloys Compd.* **2002**, *341*, 183.
(29) Hreniak, D.; Fedyk, R.; Bednarkiewicz, A.; Stręk, W.; Lojkowski, W. *Opt. Mater.* **2007**, *29*, 1244.

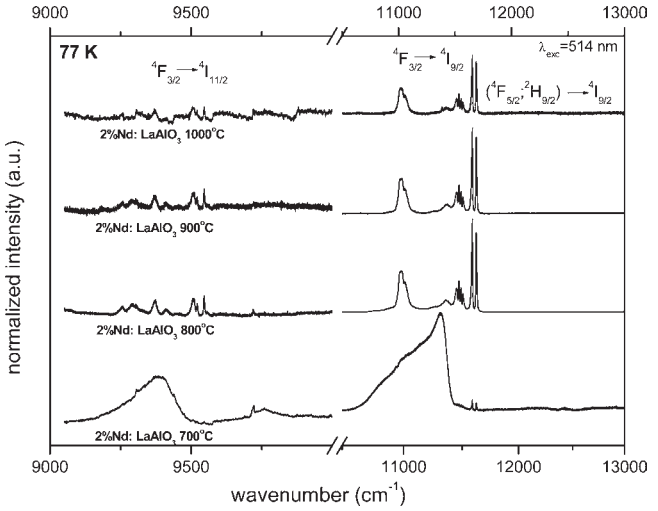

Figure 13. Luminescence spectra of the Nd:$LaAlO_3$ recorded at 77 K as a function of the sintering temperature.

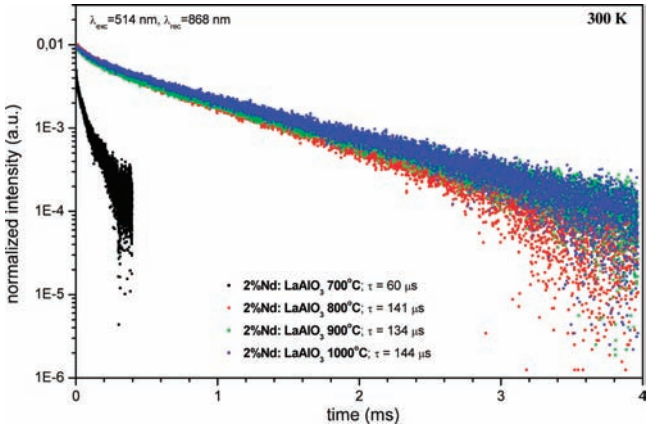

Figure 14. Decay profiles of the Nd:$LaAlO_3$ measured at 300 K.

sample and/or coexistence of the crystalline particles among the amorphous parts (confirmed by TEM observations). Results of the luminescence kinetics studies showed nonexponential profiles of the decay times (see Figure 14). Thus, for calculation of the lifetimes, we utilized following formula:

$$\tau_{\text{eff}} = \frac{\int_0^{\max} tI(t)\,\mathrm{d}t}{\int_0^{\max} I(t)\,\mathrm{d}t}$$

where $I(t)$ represents the luminescence intensity at time t corrected for the background, and the integrals are evaluated in a range $0 < t < t^{\max}$, where $t^{\max} \gg \tau_{\text{eff}}$.[30] Generally, the luminescence lifetimes were in the same range, being close to 140 μs, for the Nd:$LaAlO_3$ samples heated in the range of temperatures 800−1000 °C. Such short times are a consequence of the relatively high concentration of the Nd^{3+} (2 mol %), which could have as a consequence the formation of the Nd^{3+} ion pairs causing quenching of the emission via cross relaxation processes.[24] Only the powder annealed at 700 °C differs significantly, having a decay time around 60 μs, pointing to the strong quenching of the luminescence caused most probably by the presence of many defects, the amorphous phase of the $LaAlO_3$ and Nd^{3+} ions aggregation facilitating the nonradiative processes.

Luminescence lifetimes were not affected by the grain size effect. However, the dominating character of the $^4F_{3/2} \rightarrow {}^4I_{9/2}$ transition is very promising for stimulated radiation emission in powders, since only one transition dominates over the rest. Additionally, the specific spectral region covering 10 900−11 700 cm^{-1} could be used for tunable ceramic lasers after decreasing of the Nd^{3+} to the optimal content.

Conclusions

In this work, the nonhydrolytic synthesis (Bradley reaction) of the highly crystalline $LaAlO_3$ nanopowders has been carried out using the single source and stable in solution $La_2Al_2(O^iPr)_{12}(^iPrOH)_2$ molecular precursor. The controlled doping with the Nd^{3+} was successfully achieved by the addition of a respective amount of the $Nd_2Al_2(O^iPr)_{12}$-$(^iPrOH)_2$ at the stage of nanoparticle synthesis. The luminescence behavior of the Nd^{3+} pointed to the high rhombohedral distortion of the $LaAlO_3$ nanopowders compared to the single crystal. Thus, the preferred energy distribution channel is the $^4F_{3/2} \rightarrow {}^4I_{9/2}$ transition instead of $^4F_{3/2} \rightarrow {}^4I_{11/2}$, resulting in relatively low intensity for the latter one. Relatively short luminescence decay times are caused by the high concentration of the optically active ions, leading to luminescence quenching by the cross-relaxation process. Nd^{3+} doped $LaAlO_3$ could be proposed as a rather promising material for the laser application, but its luminescence properties require further tailoring.

Acknowledgment. The authors express their sincerest gratitude to Dr. Andreas Fischer for the assistance with the low temperature X-ray single crystal data collection and Dr. Corine Sandström for the help with 2-dimensional NMR experiments. The Faculty of Natural Resources, SLU is acknowledged for the support of the project "Nanoparticles for Biological and Medical Diagnostics". Swedish Research Council (Vetenskapsrådet) is gratefully acknowledged for the financial support of the project "Molecular Precursors and Molecular Models of Nanoporous Materials".

(30) Nakazawa E. In *Phosphor Handbook*; Shionoya, S., Yen, W. M., Eds.; CRC Press: Boca Raton, FL, 1999; p 104.